Inorganic Chemistry

Article

Heterospin Systems Constructed from [Cu$_2$Ln]$^{3+}$ and [Ni(mnt)$_2$]$^{1-,2-}$ Tectons: First 3p–3d–4f Complexes (mnt = Maleonitriledithiolato)[♦]

Augustin M. Madalan,[†,§] Narcis Avarvari,*,[§] Marc Fourmigué,*,[‡] Rodolphe Clérac,[⊥] Liviu F. Chibotaru,[#] Sergiu Clima,[#] and Marius Andruh*,[†]

Inorganic Chemistry Laboratory, Faculty of Chemistry, University of Bucharest, Strausse Dumbrava Rosie nr. 23, 020464 Bucharest, Romania, Laboratoire Chimie, Ingénierie Moléculaire et Matériaux (CIMMA), UMR 6200 CNRS-Université d'Angers, UFR Sciences, Bât. K, 2 Bd. Lavoisier, 49045 Angers, France, Sciences Chimiques de Rennes, UMR 6226 CNRS-Université Rennes 1, Equipe Matière Condensée et Systèmes Electroactifs (MaCSE), Bât. 10C, Campus de Beaulieu, 35042 Rennes, France, Université Bordeaux 1, CNRS, Centre de Recherche Paul Pascal (CRPP) UPR8641, 115 avenue du Dr. A. Schweitzer, 33600 Pessac, France, and University of Leuven, Division of Quantum and Chemistry, Celestijnenlaan 200F, 3001 Heverlee, Belgium

New heterospin complexes have been obtained by combining the binuclear complexes [{Cu(H$_2$O)L^1}Ln(O$_2$NO)$_3$] or [{CuL^2}Ln(O$_2$NO)$_3$] (L^1 = *N,N′*-propylene-di(3-methoxysalicylideneiminato); L^2 = *N,N′*-ethylene-di(3-methoxysalicylide-neiminato); Ln = Gd^{3+}, Sm^{3+}, Tb^{3+}), with the mononuclear [CuL$^{1(2)}$] and the nickel dithiolene complexes [Ni(mnt)$_2$]$^{q-}$ (*q* = 1, 2; mnt = maleonitriledithiolate), as follows: $^1_\infty$[{CuL^1}$_2$Ln(O$_2$NO){Ni(mnt)$_2$}]·Solv·CH$_3$CN (Ln = Gd^{3+}, Solv = CH$_3$OH (**1**), Ln = Sm^{3+}, Solv = CH$_3$CN (**2**)) and [{(CH$_3$OH)CuL^2}$_2$Sm(O$_2$NO)][Ni(mnt)$_2$] (**3**) with [Ni(mnt)$_2$]$^{2-}$, [{(CH$_3$-CN)CuL^1}$_2$Ln(H$_2$O)][Ni(mnt)$_2$]$_3$·2CH$_3$CN (Ln = Gd^{3+} (**4**), Sm^{3+} (**5**), Tb^{3+} (**6**)), and [{(CH$_3$OH)CuL^2}{CuL^2}Gd(O$_2$NO)-{Ni(mnt)$_2$}][Ni(mnt)$_2$]·CH$_2$Cl$_2$ (**7**) with [Ni(mnt)$_2$]$^{•-}$. Trinuclear, almost linear, [CuLnCu] motifs are found in all the compounds. In the isostructural **1** and **2**, two trans cyano groups from a [Ni(mnt)$_2$]$^{2-}$ unit bridge two trimetallic nodes through axial coordination to the Cu centers, thus leading to the establishment of infinite chains. **3** is an ionic compound, containing discrete [{(CH$_3$OH)CuL^2}$_2$Sm(O$_2$NO)]$^{2+}$ cations and [Ni(mnt)$_2$]$^{2-}$ anions. Within the series **4**–**6**, layers of discrete [CuLnCu]$^{3+}$ motifs alternate with stacks of interacting [Ni(mnt)$_2$]$^{•-}$ radical anions, for which two overlap modes, providing two different types of stacks, can be disclosed. The strength of the intermolecular interactions between the open-shell species is estimated through extended Hückel calculations. In compound **7**, [Ni(mnt)$_2$]$^{•-}$ radical anions coordinate group one of the Cu centers of a trinuclear [Cu$_2$Gd] motif through a CN, while discrete [Ni(mnt)$_2$]$^{•-}$ units are also present, overlapping in between, but also with the coordinated ones. Furthermore, the [Cu$_2$Gd] moieties dimerize each other upon linkage by two nitrato groups, both acting as chelate toward the gadolinium ion from one unit and monodentate toward a Cu ion from the other unit. The magnetic properties of the gadolinium-containing complexes have been determined. Ferromagnetic exchange interactions within the trinuclear [Cu$_2$Gd] motifs occur. In the compounds **4** and **7**, the [Ni(mnt)$_2$]$^{•-}$ radical anions contribution to the magnetization is clearly observed in the high-temperature regime, and most of it vanishes upon temperature decrease, very likely because of the rather strong antiferromagnetic exchange interactions between the open-shell species. The extent of the exchange interaction in the compound **7**, which was found to be antiferromagnetic, between the coordinated Cu center and the corresponding [Ni(mnt)$_2$]$^{•-}$ radical anion, bearing mostly a 3p spin type, was estimated through CASSCF/CASPT2 calculations. Compound **6** exhibits a slow relaxation of the magnetization.

Introduction

The tremendous development of molecular magnetism has stimulated, over the last 20 years, the synthesis of a plethora of heterometallic complexes, ranging from oligonuclear clusters to three-dimensional (3-D) coordination polymers.[1] The combination of metal ions carrying different spins emphasized important concepts in molecular magnetism, such as irregular spin-state structure and one-dimensional (1-D) systems with a ferrimagnetic spin arrangement.[1] The ferromagnetic coupling arising from the orthogonality of the magnetic orbitals was illustrated by a famous heterobinuclear Cu^{II}−VO^{II} complex.[2] One of the very first molecular

[♦] Dedicated to Professor Achim Müller on the occasion of his 70th birthday.

* Author to whom correspondence should be addressed. E-mail: marius.andruh@dnt.ro.

[†] University of Bucharest.

[§] CNRS-Université d'Angers.

[‡] CNRS-Université Rennes 1.

[⊥] Université Bordeaux 1, CNRS, CRPP.

[#] University of Leuven.

(1) (a) Kahn, O. *Struct. Bond. (Berlin)* **1987**, *68*, 89 (b) Kahn, O. *Adv. Inorg. Chem.* **1995**, *43*, 179.

(2) Kahn, O.; Galy, J.; Journaux, Y. *J. Am. Chem. Soc.* **1982**, *104*, 2165.

magnets, synthesized by Kahn and co-workers, contained two different 3d metal ions: Cu^{2+} (d^9) and Mn^{2+} (d^5).[3] In the same year, Miller et al.[4] reported on a new molecular magnet that is a supramolecular system constructed from tectons bearing a 3d electron, $[FeCp^*_2]^{\bullet+}$, and a 2p electron, $TCNE^{\bullet-}$ (Cp^{*-} = pentamethylcyclopentadienyl anion; TCNE = tetracyanoethylene). Several years later, a molecule-based magnet with a unique interlocked structure was obtained by associating two different 3d metal ions (Mn^{2+} and Cu^{2+}) and a radical (2p) cation.[5] Most of the single-chain magnets reported to date are constructed from different spin carriers.[6] Many other systems exhibiting interesting magnetic properties are based on the following pairs of spin carriers: 3d−4d,[7] 3d−5d,[8] 3d−4f,[9] 3d−5f,[10] 3d−Rad$^{\bullet}$,[11] and 4f−Rad$^{\bullet}$.[12] In contrast, the number of the polynuclear complexes containing three different metal ions, all of them paramagnetic, is limited to only few examples. The first trimetallic 3d−3d′−3d″ complexes were reported by Chaudhuri et al.[13] Their synthetic approach is based on the use of bicompartmental ligands functionalized with oximato groups, which coordinate to the third metal ion.

We recently developed an alternative method to obtain 3d−3d′−4f heterotrimetallics.[14] It relies on binuclear Cu^{II}−Ln^{III} complexes with compartmental side-off ligands derived from 3-methoxy-salicylaldehyde and a diamine. Such ligands were specially designed by Costes, some 10 years ago, to obtain heterobinuclear 3d−4f complexes.[15] The third paramagnetic metal ion arises from an anionic complex with potentially bridging ligands, that is, a metalloligand, which can coordinate either to the 3d ion, to the lanthanide one, or even, to both of them. Such metalloligands are, for example, the hexacyano complexes $[M(CN)_6]^{3-}$. The self-assembly process between $[L^1CuLn]^{3+}$ and $[M(CN)_6]^{3-}$ ions has led to a family of isomorphous complexes, $[\{L^1Cu\}Ln(H_2O)_3\{M(CN)_6\}]\cdot4H_2O$ (M = Cr^{III}, Fe^{III}, Co^{III}, L^1 is the dianion of the Schiff-base resulted from the 2:1 condensation of 3-methoxy-salicylaldehyde with propylenediamine). The $[M(CN)_6]^{3-}$ ion connects three metal ions (two Cu^{II} and one Ln^{III}) through three meridially disposed cyano groups, resulting in a ladder-type topology.[14]

The third spin carrier can be a radical as well. Numerous organic radicals are able to coordinate to metal centers.[16] We recently described a 2p($TCNQ^{\bullet-}$)−3d(Cu^{2+})−4f(Gd^{3+}) heterospin complex, $[\{CuL^1\}_2Gd(TCNQ)_2]\cdot(TCNQ)\cdot(CH_3OH)\cdot2CH_3CN$, which has been obtained by reacting the mononuclear precursor, $[CuL^1]$, with gadolinium nitrate and LiTCNQ ($TCNQ^{\bullet-}$ = the radical anion of 7,7,8,8-tetracyano-*p*-quinodimethane).[17]

The chemistry of bis(dithiolene) complexes represents a very active area of research because of their exciting conducting, magnetic, optical, and catalytic properties.[18] The complexes obtained by using maleonitriledithiolate (mnt) ligands are among the most popular from this family.[18,19] The bis(mnt) species, $[M(mnt)_2]^{q-}$ (M = Ni, Pd, Pt, q = 1; 2), display a planar structure that favors a highly delocalized electronic structure. The cyano groups confer to these complexes an extremely versatile behavior. These groups are able to sustain supramolecular solid-state architectures through (a) hydrogen-bond interactions,[20] (b) CN···Hal interactions,[21] and (c) coordinative bonds, forming heterometallic complexes.[22] The most interesting from the magnetic point of view are the q = −1 derivatives because of their paramagnetism (S = 1/2). The $[M(mnt)_2]^{\bullet-}$ species, carrying an unpaired electron and being potentially able to coordinate through the cyano groups to another metal ion, are thus very appealing candidates in the attempt to obtain novel heterospin complexes. In this paper, we report the first systems constructed by employing 3d−4f and $[Ni(mnt)_2]^{q-}$ building blocks.

(3) Pei, Y.; Verdaguer, M.; Kahn, O.; Sletten, J.; Renard, J.-P. *J. Am. Chem. Soc.* **1986**, *108*, 428.

(4) Miller, J. S.; Calabrese, J. C.; Epstein, A. J.; Bigelow, R. W.; Zhang, J. H.; Reiff, W. M. *J. Chem. Soc., Chem. Commun.* **1986**, 1026.

(5) Stumpf, H. O.; Ouahab, L.; Pei, Y.; Grandjean, D.; Kahn, O. *Science* **1993**, *261*, 447.

(6) (a) Caneschi, A.; Gatteschi, D.; Lalioti, N.; Sangregario, C.; Sessoli, R.; Venturi, G.; Vindigni, A.; Rettori, A.; Pini, M. G.; Novak, M. A. *Angew. Chem., Int. Ed.* **2001**, *40*, 1760. (b) Clérac, R.; Miyasaka, H.; Yamashita, M.; Coulon, C. *J. Am. Chem. Soc.* **2002**, *124*, 12837. (c) Lescouëzec, R.; Toma, L. M.; Vaissermann, J.; Verdaguer, M.; Delgado, F. S.; Ruiz-Pérez, C.; Lloret, F.; Julve, M. *Coord. Chem. Rev.* **2005**, *249*, 2691. (d) Coulon, C.; Miyasaka, H.; Clérac, R. *Struct. Bond.* **2006**, *122*, 163.

(7) For example, see: (a) Kahn, O.; Larionova, J.; Ouahab, L. *Chem. Commun.* **1999**, 945 and references therein. (b) Visinescu, D.; Desplanches, C.; Imaz, I.; Bahers, V.; Pradhan, R.; Villamena, F. A.; Guionneau, P.; Sutter, J.-P. *J. Am. Chem. Soc.* **2006**, *128*, 10202.

(8) For example, see: (a) Zhong, Z. J.; Seino, H.; Mizobe, Y.; Hidai, M.; Fujishima, A.; Ohkoshi, S.; Hashimoto, K. *J. Am. Chem. Soc.* **2000**, *122*, 2952. (b) Sieklucka, B.; Podgajny, R.; Przychodzen, P.; Korzeniak, T. *Coord. Chem. Rev.* **2005**, *249*, 2203.

(9) For example, see: Sakamoto, M.; Manseki, K.; Okawa, H. *Coord. Chem. Rev.* **2001**, *219−221*, 379 and references therein.

(10) For example, see: (a) Le Borgne, T.; Rivière, E.; Marrot, J.; Girerd, J.-J.; Ephritikhine, M. *Angew. Chem., Int. Ed.* **2000**, *39*, 1647. (b) Mishra, A.; Abboud, K. A.; Christou, G. *Inorg. Chem.* **2006**, *45*, 2364.

(11) For example, see: (a) Fegy, K.; Luneau, D.; Ohm, T.; Paulsen, C.; Rey, P. *Angew. Chem., Int. Ed.* **1998**, *37*, 1270. (b) Kumagai, H.; Inoue, K. *Angew. Chem., Int. Ed.* **1999**, *38*, 1601. (c) Fujita, W.; Awaga, K. *J. Am. Chem. Soc.* **2001**, *123*, 3601. (d) Luneau, D.; Rey, P. *Coord. Chem. Rev.* **2005**, *249*, 2591.

(12) For example, see: (a) Sutter, J.-P.; Kahn, M. L.; Golhen, S.; Ouahab, L.; Kahn, O. *Chem.−Eur. J.* **1998**, *4*, 571. (b) Lescop, C.; Luneau, D.; Belorizky, E.; Guillot, M.; Rey, P. *Inorg. Chem,* **1999**, *38*, 5472. (c) Zhao, H.; Bazile, Jr., M. J.; J. Galán−Mascarós, R.; Dunbar, K. R. *Angew. Chem., Int. Ed.* **2003**, *42*, 1015.

(13) (a) Verani, C. N.; Weyhermüller, T.; Rentschler, E.; Bill, E.; Chaudhuri, P. *Chem. Commun.* **1998**, 2475. (b) Verani, C. N.; Rentschler, E.; Weyhermüller, T.; Bill, E.; Chaudhuri, P. *J. Chem. Soc., Dalton Trans.* **2000**, 4263.

(14) (a) Gheorghe, R.; Andruh, M.; Costes, J.-P.; Donnadieu, B. *Chem. Commun.* **2003**, 2778. (b) Gheorghe, R.; Cucos, P.; Andruh, M.; Costes, J.-P.; Donnadieu, B.; Shova, S. *Chem.−Eur. J.* **2006**, *12*, 187.

(15) Costes, J.-P.; Dahan, F.; Dupuis, A.; Laurent, J.-P. *Inorg. Chem.* **1996**, *35*, 2400.

(16) Blundell, S. J.; Pratt, F. L. *J. Phys., Condens. Mater.* **2004**, *16*, R771.

(17) Madalan, A. M.; Roesky, H. W.; Andruh, M.; Noltemeyer, M.; Stanica, N. *Chem. Commun.* **2002**, 1638.

(18) (a) Robertson, N.; Cronin, L. *Coord. Chem. Rev.* **2002**, *227*, 93. (b) Kato, R. *Chem. Rev.* **2004**, *104*, 5319.

(19) Clemenson, P. I. *Coord. Chem. Rev.* **1990**, *106*, 171.

(20) For example, see: (a) Fourmigué, M.; Mézière, C.; Dolou, S. *Cryst. Growth Des.* **2003**, *3*, 805. (b) Ren, X. M.; Nishihara, S.; Akutagawa, T.; Noro, S.; Nakamura, T. *Inorg. Chem.* **2006**, *45*, 2229.

(21) (a) Nishijo, J.; Ogura, E.; Yamaura, J.; Miyazaki, A.; Enoki, T.; Takano, T.; Kuwatani, Y.; Iyoda, M. *Solid State Commun.* **2000**, *116*, 661. (b) Devic, T.; Domercq, B.; Auban-Senzier, P.; Molinié, P.; Fourmigué, M. *Eur. J. Inorg. Chem.* **2002**, 2844.

(22) For example, see: Dawe, L. N.; Miglioli, J.; Turnbow, L.; Taliaferro, M. L.; Shum, W. W.; Bagnato, J. B.; Zakharov, L. N.; Rheingold, A. L.; Arif, A. M.; Fourmigué, M.; Miller, J. S. *Inorg. Chem.* **2005**, *44*, 7530.

Results and Discussion

Our synthetic approach relies upon assembly processes involving 3d−4f complex cations and $[Ni(mnt)_2]^{q-}$ anions. The reaction between the mononuclear precursors, $[Cu(H_2O)L^1]/[CuL^2]$, and rare earth nitrates usually leads to binuclear complexes, $[\{Cu(H_2O)L^1\}Ln(O_2NO)_3]$ and $[\{CuL^1\}Ln(O_2NO)_3]$, but trinuclear $[\{CuL^{1(2)}\}_2Ln]^{3+}$ species can be assembled as well $[L^1 = N,N'$-propylene-di(3-methoxysalicylideneiminato), $L^2 = N,N'$-ethylene-di(3-methoxysalicylideneiminato)].[14b,17,23]
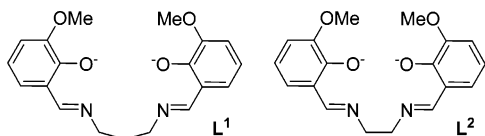
Both $[\{CuL^{1(2)}\}Ln]^{3+}$ and $[\{CuL^{1(2)}\}_2Ln]^{3+}$ species are useful precursors in designing heterometallic assemblies.[14,17,24] The $[Ni(mnt)_2]^{q-}$ ions can act either as monodentate or as bridging ligands. They can also be found uncoordinated, counterbalancing the charge of the complex cations. An important peculiar behavior of the $[Ni(mnt)_2]^{q-}$ ions is represented by the interplay between the Ni···Ni, Ni···S, and S···S interactions established between neighboring $[Ni(mnt)_2]^{q-}$ ions through orbital overlap, thus affording direct exchange interactions in the case of paramagnetic species. Such interactions lead to interesting supramolecular solid-state architectures and strongly influence the magnetic properties.[18,19]

1-D Coordination Polymers by Connecting [Cu₂Ln] Nodes with [Ni(mnt)₂]²⁻ Spacers. The reaction between the neutral mononuclear copper complex $[Cu(H_2O)L^1]$, the binuclear complex $[\{Cu(H_2O)L^1\}Ln(O_2NO)_3]$ (Ln = Gd^{3+}, Sm^{3+}), and $(TBA)_2[Ni(mnt)_2]$ (TBA = n-tetrabutylammonium) affords the 1-D coordination polymers $^1_\infty[\{CuL^1\}_2Gd(O_2NO)\{Ni(mnt)_2\}]\cdot CH_3OH\cdot CH_3CN$ (**1**) and $^1_\infty[\{CuL^1\}_2Sm(O_2NO)\{Ni(mnt)_2\}]\cdot 2CH_3CN$ (**2**). The structure of **1** (Figure 1) is constructed from almost linear trinuclear [Cu₂Gd] units, which are connected through $[Ni(mnt)_2]^{2-}$ bridges (the value of the Cu−Gd−Cu angle is 176.9°). The $[Ni(mnt)_2]^{2-}$ ion coordinates through two trans cyano groups into the apical positions of two copper ions belonging to two [Cu₂Gd] nodes, thus affording zigzag chains. The distance between the copper and gadolinium ions within a node is 3.4605(4) Å. The copper(II) ions are pentacoordinated with a square-pyramidal geometry. The basal positions are occupied by the oxygen and nitrogen atoms from the compartmental ligand, while the apical position is occupied by the nitrogen atom arising from the CN group [Cu1−N4 = 2.428(4) Å]. The coordination number of the gadolinium ion is ten: eight oxygen atoms from two organic ligands and two oxygen atoms from the chelating nitrato ligand. The
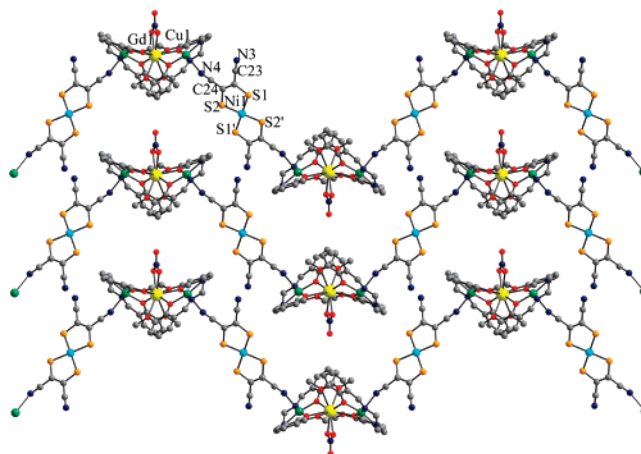
Figure 1. Perspective view of chains in compound **1**, along with the atom numbering scheme.

Gd−O distances vary between 2.345(2) and 2.745(2) Å. The short distances correspond to the Gd−O(phenoxo) bonds, while the long ones to the Gd−O(methoxy) bonds.

The bridging $[Ni(mnt)_2]^{2-}$ units are perfectly planar. The Ni−S distances (average of 2.170 Å) are in good agreement with those observed for other compounds containing the $[Ni(mnt)_2]^{2-}$ ion.[25,26] The C≡N distance of 1.147(5) Å from the nitrile group coordinated to the copper ion is slightly larger than the one found for the uncoordinated CN group, 1.133(6) Å. Selected bond distances are presented in Table 1. The samarium derivative, $^1_\infty[\{CuL^1\}_2Sm(O_2NO)\{Ni(mnt)_2\}]\cdot 2CH_3CN$ **2**, was found to be isostructural with compound **1**.

Ionic Compound Constructed from $[\{CuL^2\}_2Ln(O_2NO)]^{2+}$ Cations and $[Ni(mnt)_2]^{2-}$ Anions. Interestingly, when the bi-compartmental ligand is changed (L^2 instead of L^1), the reaction between the neutral mononuclear copper complex, $[CuL^2]$, the binuclear complex, $[\{CuL^2\}Sm(O_2NO)_3]$, and $(TBA)_2[Ni(mnt)_2]$ afforded $[\{(CH_3OH)CuL^2\}_2Sm(O_2NO)][Ni(mnt)_2]$, **3**, an ionic compound that is formed by discrete $[\{(CH_3OH)CuL^2\}_2Sm(O_2NO)]^{2+}$ cations and $[Ni(mnt)_2]^{2-}$ anions (Figure 2). The organic ligand, H_2L^2, is slightly modified, being obtained from ethylenediamine, instead of 1,3-propanediamine, and 3-methoxy-salicylaldehyde. Thus, the substitution of the ethylene linker for the propylene one in the structure of the Schiff base induced here a completely different crystal structure, as observed in other cases.[27] Within the trinuclear $[\{(CH_3OH)CuL^2\}_2Sm(O_2NO)]^{2+}$ moieties, the copper(II) ions exhibit a square-pyramidal stereochemistry with the basal positions occupied by the oxygen and nitrogen atoms from the compartmental ligand and a methanol molecule coordinated into the apical position [Cu1−O12 = 2.418(4) Å, Cu2−O13 = 2.402(4) Å] (see Table 1). In a manner similar to that of compounds **1** and **2**, the coordination sphere of the samarium ion is built

(23) Costes, J.-P.; Dahan, F.; Dupuis, A.; Laurent, J.-P. *New J. Chem.* **1998**, 1525.
(24) (a) Andruh, M. *Chem. Commun.* **2007**, 2565. (b) Gheorghe, R.; Andruh, M.; Müller, A.; Schmidtmann, M. *Inorg. Chem.* **2002**, *41*, 5314. (c) Novitchi, G.; Costes, J.-P.; Donnadieu, B. *Eur. J. Inorg. Chem.* **2004**, 1808. (d) Costes, J.-P.; Novitchi, G.; Shova, S.; Dahan, F.; Donnadieu, B.; Tuchagues, J.-P. *Inorg. Chem.* **2004**, *43*, 7792.
(25) Pullen, A. E.; Faulmann, C.; Pokhodnya, K. I.; Cassoux, P.; Takumoto, M. *Inorg. Chem.* **1998**, *37*, 6714.
(26) Dang, D.; Bai, Y.; Wen, L.; Tian, Z.; Li, Meng, Y., Q. *J. Mol. Struct.* **2005**, *753*, 99.
(27) Kitagawa, S.; Noro, S. In *Comprehensive Coordination Chemistry II*; McCleverty, J. A., Meyer, T. J., Eds.; Elsevier: Amsterdam, 2004; Vol. 7, p. 231.

Table 1. Selected Geometric Parameters of Coordination Surroundings of the Metal Ions[a]

1	2	3	
Cu1−O2 = 1.955(2)	Cu1−O2 = 1.962(2)	Cu1−O2 = 1.912(3)	Cu2−O6 = 1.920(3)
Cu1−O3 = 1.949(2)	Cu1−O3 = 1.952(2)	Cu1−O4 = 1.915(3)	Cu2−O7 = 1.921(3)
Cu1−N1 = 1.966(3)	Cu1−N1 = 1.974(3)	Cu1−O12 = 2.418(4)	Cu2−O13 = 2.402(4)
Cu1−N2 = 1.957(3)	Cu1−N2 = 1.965(3)	Cu1−N1 = 1.917(4)	Cu2−N3 = 1.922(4)
Cu1−N4 = 2.428(4)	Cu1−N4 = 2.443(4)	Cu1−N2 = 1.929(4)	Cu2−N4 = 1.932(3)
Gd1−O1 = 2.619(2)	Sm1−O1 = 2.636(2)	Sm1−O1 = 2.715(3)	Sm1−O6 = 2.505(3)
Gd1−O2 = 2.3446(19)	Sm1−O2 = 2.363(2)	Sm1−O2 = 2.448(3)	Sm1−O7 = 2.351(3)
Gd1−O3 = 2.370(2)	Sm1−O3 = 2.389(2)	Sm1−O3 = 2.636(3)	Sm1−O8 = 2.626(3)
Gd1−O4 = 2.745(2)	Sm1−O4 = 2.750(2)	Sm1−O4 = 2.395(3)	Sm1−O9 = 2.502(4)
Gd1−O5 = 2.509(3)	Sm1−O5 = 2.536(3)	Sm1−O5 = 2.645(3)	Sm1−O10 = 2.510(4)
Ni1−S1 = 2.1689(10)	Ni1−S1 = 2.1690(9)	Ni-S1 = 2.1714(14)	Ni-S3 = 2.1685(13)
Ni1−S2 = 2.1714(9)	Ni1−S2 = 2.1789(10)	Ni-S2 = 2.1753(14)	Ni-S4 = 2.1774(14)

4	5	6	7
Cu1−N1 = 1.987(6)	Cu1−N1 = 1.959(8)	Cu1−N1 = 1.996(13)	Cu1−N1 = 1.920(6)
Cu1−N2 = 1.957(7)	Cu1−N2 = 1.960(7)	Cu1−N2 = 1.965(13)	Cu1−N2 = 1.907(6)
Cu1−N2S = 2.342(8)	Cu1−N2S = 2.356(10)	Cu1−N2S = 2.300(19)	Cu1−O2 = 1.908(4)
Cu1−O2 = 1.948(4)	Cu1−O2 = 1.931(5)	Cu1−O2 = 1.923(9)	Cu1−O4 = 1.916(4)
Cu1−O4 = 1.954(5)	Cu1−O4 = 1.944(6)	Cu1−O4 = 1.962(9)	Cu1−O1S = 2.473(13)
Cu2−N3 = 1.973(7)	Cu2−N3 = 1.962(8)	Cu2−N3 = 1.928(15)	Cu2−N3 = 1.888(5)
Cu2−N4 = 1.952(7)	Cu2−N4 = 1.962(8)	Cu2−N4 = 2.004(14)	Cu2−N4 = 1.913(5)
Cu2−N1S = 2.538(13)	Cu2−N1S = 2.541(16)	Cu2−N1S = 2.45(2)	Cu2−O6 = 1.902(4)
Cu2−O6 = 1.945(5)	Cu2−O6 = 1.937(6)	Cu2−O6 = 1.957(9)	Cu2−O8 = 1.908(4)
Cu2−O8 = 1.960(5)	Cu2−O8 = 1.948(6)	Cu2−O8 = 1.943(11)	Cu2−N8 = 2.792(13)
Gd1−O1 = 2.498(4)	Sm1−O1 = 2.513(5)	Tb1−O1 = 2.483(10)	Gd1−O1 = 2.724(5)
Gd1−O2 = 2.367(4)	Sm1−O2 = 2.376(5)	Tb1−O2 = 2.343(9)	Gd1−O2 = 2.416(4)
Gd1−O3 = 2.562(5)	Sm1−O3 = 2.556(5)	Tb1−O3 = 2.587(9)	Gd1−O3 = 2.572(4)
Gd1−O4 = 2.417(5)	Sm1−O4 = 2.437(5)	Tb1−O4 = 2.400(9)	Gd1−O4 = 2.330(4)
Gd1−O5 = 2.573(5)	Sm1−O5 = 2.598(5)	Tb1−O5 = 2.587(11)	Gd1−O5 = 2.850(4)
Gd1−O6 = 2.439(5)	Sm1−O6 = 2.446(5)	Tb1−O6 = 2.386(10)	Gd1−O6 = 2.418(3)
Gd1−O7 = 2.499(5)	Sm1−O7 = 2.544(6)	Tb1−O7 = 2.470(12)	Gd1−O7 = 2.659(4)
Gd1−O8 = 2.369(5)	Sm1−O8 = 2.389(5)	Tb1−O8 = 2.354(10)	Gd1−O8 = 2.342(4)
Gd1−O1W = 2.380(4)	Sm1−O1W = 2.391(6)	Tb1−O1W = 2.335(11)	Gd1−O9 = 2.475(7)
Ni1−S1 = 2.144(2)	Ni1−S1 = 2.142(3)	Ni1−S1 = 2.141(5)	Gd1−O10 = 2.447(7)
Ni1−S2 = 2.153(3)	Ni1−S2 = 2.153(3)	Ni1−S2 = 2.158(5)	Ni1−S1 = 2.1475(17)
Ni1−S3 = 2.149(2)	Ni1−S3 = 2.145(3)	Ni1−S3 = 2.138(5)	Ni1−S2 = 2.146(2)
Ni1−S4 = 2.137(3)	Ni1−S4 = 2.141(3)	Ni1−S4 = 2.138(5)	Ni1−S3 = 2.1560(18)
Ni2−S5 = 2.150(2)	Ni2−S5 = 2.153(3)	Ni2−S5 = 2.163(5)	Ni1−S4 = 2.139(2)
Ni2−S6 = 2.147(2)	Ni2−S6 = 2.152(3)	Ni2−S6 = 2.154(5)	Ni2−S5 = 2.139(2)
Ni2−S7 = 2.156(2)	Ni2−S7 = 2.155(3)	Ni2−S7 = 2.154(5)	Ni2−S6 = 2.139(2)
Ni2−S8 = 2.156(2)	Ni2−S8 = 2.152(3)	Ni2−S8 = 2.151(5)	Ni2−S7 = 2.128(2)
Ni3−S9 = 2.145(2)	Ni3−S9 = 2.143(3)	Ni3−S9 = 2.149(5)	Ni2−S8 = 2.139(2)
Ni3−S10 = 2.141(2)	Ni3−S10 = 2.139(3)	Ni3−S10 = 2.147(5)	
Ni4−S11 = 2.147(2)	Ni4−S11 = 2.149(3)	Ni4−S11 = 2.161(4)	
Ni4−S12 = 2.155(2)	Ni4−S12 = 2.153(2)	Ni4−S12 = 2.153(5)	

[a] Bond Lengths (Å) for Compounds 1−7.
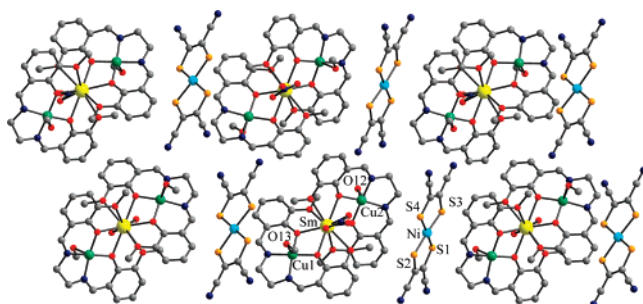
Figure 2. View of the ionic entities in crystal **3**, along with the atom numbering scheme.

by ten oxygen atoms, eight from the compartmental ligands and two from a chelating nitrato anion. In crystal **3**, the planar anions [Ni(mnt)$_2$]$^{2-}$ are isolated from each other.

Supramolecular Systems Constructed from Three Different Spin Carriers. The interaction between [{CuL^1}$_2$-Gd]$^{3+}$ and [Ni(mnt)$_2$]$^{\bullet-}$ ions leads to an ionic compound, [{(CH$_3$CN)CuL^1}$_2$Gd(H$_2$O)][Ni(mnt)$_2$]$_3$·2CH$_3$CN, **4**, whose structure consists of [Cu$_2$Gd]$^{3+}$ cations and [Ni(mnt)$_2$]$^-$

anions. The trinuclear cations are almost linear with the Cu−Gd−Cu angle of 177.5°. Each copper ion displays a square pyramidal geometry with one acetonitrile molecule coordinated into the apical position [Cu1−N2S = 2.342(8) Å, Cu2−N1S = 2.538(13) Å] (Figure 3).

The coordination number of gadolinium is nine: eight O atoms arising from two compartmental ligands and one aqua ligand. The Gd−O distances vary between 2.367(4) and 2.573(5) Å. The Cu···Gd distances are 3.544(3) and 3.540-(3) Å. The water molecule coordinated to the gadolinium-(III) ion is involved in hydrogen-bonding interactions with the uncoordinated acetonitrile molecules [O1W···N3S = 2.809(11) Å, O1W···N4S = 2.663(17) Å; Figure 3]. There are four crystallographically independent nickel atoms (Ni1, Ni2, Ni3, Ni4), of which Ni3 and Ni4 are on inversion centers. The Ni−S distances vary between 2.137(5) and 2.156(3) Å, being slightly shorter than those found in the corresponding dianion, as observed with similar com-
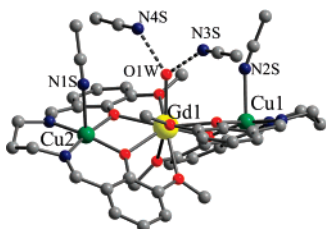
Figure 3. View of the cationic trinuclear unit and of the hydrogen-bond interactions in crystal **4**.

pounds,[26,28] a likely consequence of the antibonding Ni–S orbital combination in the HOMO of $[Ni(mnt)_2]^{2-}$. The analysis of the packing diagram of the anions reveals interesting features. The anions organize in two distinct columns, both running along the crystallographic axis *a*: one column is formed by Ni1 and Ni3 ions, while the other is formed by Ni2 and Ni4 ions (Figure 4a).

The stacking mode, interaction energies, and orientation of the anions in the two columns are not similar, even though both can be considered as stacking of triads {Ni1Ni3Ni1} and {Ni2Ni4Ni2}, respectively. In the first column, one can observe overlaps between Ni1 and Ni3 molecules, characterized by slight longitudinal and transversal offsets (Figure 4b), leading to the establishment of rather short intermolecular Ni⋯S contacts of 3.627 (Ni1⋯S10) and 3.527 Å (Ni3⋯S3), with the Ni1⋯Ni3 distance amounting to 4.023 Å. The strength of this interaction, amounting to 0.245 eV (interaction **I**), is estimated through the $\beta_{HOMO-HOMO}$ interaction energy calculated with the extended Hückel method.[29] Moreover, despite the massive longitudinal shift, corresponding to a Ni1⋯Ni1′ $(1 - x, -1 - y, 1 - z)$ distance of 6.197 Å (Figure 4c), there is also a favorable overlap between the neighboring Ni1 units, for which the calculated $\beta_{HOMO-HOMO}$ interaction energy amounts to 0.415 eV (interaction **II**), that is, 0.17 eV larger than the Ni1–Ni3 interaction I. In the second column, Ni2⋯Ni2′ $(1 - x, 1 - y, 2 - z)$ dyads and Ni4 molecules stack in a peculiar criss-cross manner, and hence, two interactions can be disclosed. The first one, corresponding to the Ni2⋯Ni2′ overlap (Figure 4d) and characterized by Ni2⋯Ni2′ $(1 - x, 1 - y, 2 - z)$ and Ni2⋯S8′ $(1 - x, 1 - y, 2 - z)$ distances of 4.150 and 3.395 Å, respectively, has a $\beta_{HOMO-HOMO}$ interaction energy of 0.090 eV (interaction **III**). Then, the Ni4 anions interact through Ni⋯S contacts with neighboring Ni2 ions (Ni4⋯S8 = 3.507 Å, Ni2⋯S12 = 3.512 Å, Ni2⋯Ni4 = 4.150 Å) (Figure 4e). The corresponding $\beta_{HOMO-HOMO}$ interaction energy amounts to 0.429 eV (interaction **IV**). It is thus clear, as far as the HOMO–HOMO interactions are concerned, that this column can be described as a uniform chain of {Ni2Ni4Ni2} triads established upon the interaction **IV**, interacting each other through the interaction **III**. Other selected bonded distances are collected in Table 1.

(28) Zhou, H.; Wen, L. L.; Ren, X. M.; Meng, Q. J. *J. Mol. Struct.* **2006**, *787*, 31 and references therein.

(29) (a) Whangbo, M.-H.; Williams, J. M.; Leung, P. C. W.; Beno, M. A.; Emge, T. J.; Wang, H. H. *Inorg. Chem.* **1985**, *24*, 3500. (b) Hoffmann, R. *J. Chem. Phys.* **1963**, *39*, 1397. (c) Beswick, C. L.; Schulman, J. M.; Stiefel, E. I. In *Progress in Inorganic Chemistry*; Karlin, K. D., Stiefel, E. I., Eds.; Wiley: New York, 2004; Vol. 52, p. 55.

The isostructural compounds [{(MeCN)CuL^1}$_2$Sm(H$_2$O)]-[Ni(mnt)$_2$]$_3$·2MeCN, **5**, and [{(MeCN)CuL^1}$_2$Tb(H$_2$O)][Ni-(mnt)$_2$]$_3$·2MeCN, **6**, have been synthesized by replacement of the gadolinium(III) ion with samarium(III) and terbium-(III), respectively. The latter has been chosen because of its strong magnetic anisotropy (as a prerequisite to obtain single molecule magnets or single chain magnets).

Genuine 3p−3d−4f Heterospin Complex, [{(CH$_3$OH)-CuL^2}{CuL^2}Gd(O$_2$NO){Ni(mnt)$_2$}][Ni(mnt)$_2$]·CH$_2$Cl$_2$, **7**. This compound was obtained by following the same general procedure as described for compounds **4−6**, by using L^2 instead of L^1. Once again, as observed within series **1−3**, the use of a different linker, that is, ethylene instead of propylene, promoted a different coordination pattern.

The crystallographic investigation of **7** reveals [{(CH$_3$-OH)CuL^2}{CuL^2}Gd(O$_2$NO){Ni(mnt)$_2$}]$_2$$^{2+}$ cationic octanuclear species, uncoordinated [Ni(mnt)$_2$]$^-$ ions, and solvent molecules. The cationic species are constructed out of two [Cu$_2$Gd] moieties bridged by two nitrato groups (each one acting as chelate toward the gadolinium ion from a unit and monodentate toward the Cu2 ion from the other unit) (Figure 5). The Cu2 ions exhibit an elongated octahedral stereochemistry because their two apical positions are occupied by a nitrato oxygen atom [Cu2−O11′ = 2.944(10) Å] and by a nitrogen atom arising from one [Ni(mnt)$_2$]$^-$ ion [Cu2−N8 = 2.792(13) Å]. Although long, the Cu2−O11′ and Cu2−N8 distances are still in the limits of the semicoordination.[30] The Cu1 ions are five-coordinated [square pyramidal geometry with a methanol molecule in the apical position, Cu1−O1S = 2.473(13) Å]. The gadolinium ion is tencoordinated (eight oxygen atoms from two [CuL^2] metalloligands and two oxygen atoms from the chelating nitrato ligand). The Gd−O distances vary between 2.331(4) and 2.852(5) Å, while the Cu1⋯Gd1 and Cu2⋯Gd1 distances are 3.427(11) and 3.417(8) Å, respectively. The value of the Cu1−Gd−Cu2 angle is 173.07°.

The [Ni(mnt)$_2$]$^-$ units are stacked in tetramers, with the semicoordinated anions embracing the uncoordinated ones (Figure 6a). Thus, the coordinated Ni1 anions overlap with the uncoordinated Ni2 anions (Figure 6b), mainly, through Ni⋯S contacts amounting to 3.639 (Ni2⋯S1) and 3.680 (Ni1⋯S5) Å. The associated $\beta_{HOMO-HOMO}$ interaction energy of 0.430 eV is indicative of a rather strong interaction between the two moieties (interaction **I**). The second interaction, **II**, arising from the Ni2⋯Ni2′ $(2 - x, 2 - y, 1 - z)$ overlap (Figure 6c) and characterized by Ni⋯S contacts of 3.666 Å, appears to be much weaker according to the value of 0.048 eV for the corresponding $\beta_{HOMO-HOMO}$ interaction. Therefore, rather strong exchange interactions between the Ni1⋯Ni2 fragments can be expected.

The bond lengths characterizing the coordination surroundings of the metal ions in compounds **1−7** are listed in Table 1.

Magnetic Properties. In this section, we will focus on the magnetic properties of the gadolinium and terbium derivatives. The magnetic behavior of the gadolinium

(30) Valach, F. *Polyhedron* **1999**, *18*, 699.

Figure 4. Packing diagram for crystal **4** (a) and details of the interactions between the [Ni(mnt)$_2$]$^-$ anions (b−e).

Figure 5. View of the cationic [{(CH$_3$OH)CuL^2}{CuL^2}Gd(O$_2$NO){Ni-(mnt)$_2$}]$_2$$^{2+}$ unit in crystal **7**.
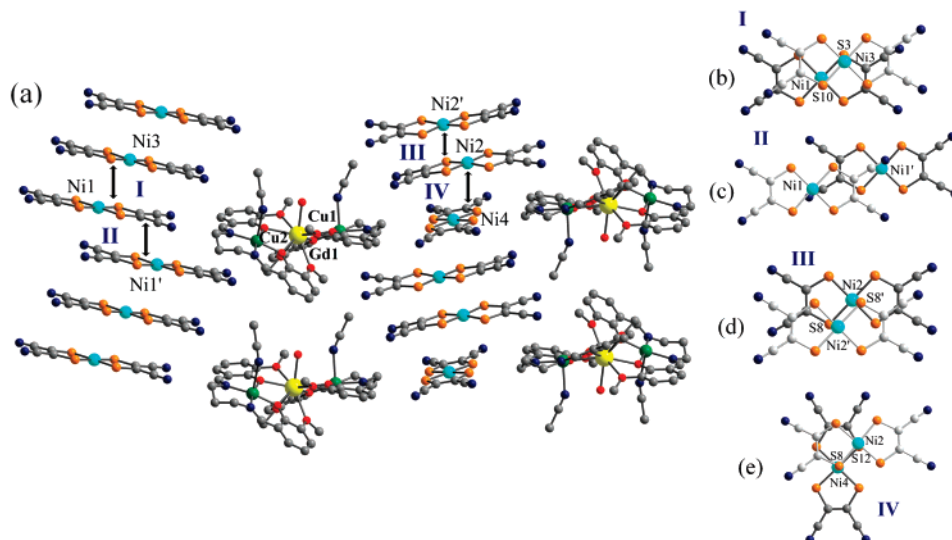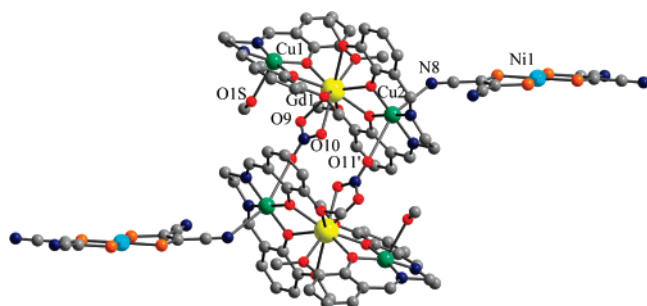
complexes can be easily analyzed by using an isotropic Heisenberg−Dirac−Van Vleck Hamiltonian, and the Cu^{II}−Gd^{III} exchange interaction can be accurately determined. The case of the terbium derivative is particularly interesting, because it could show a slow relaxation of the magnetization. The temperature dependence of χT for **1** is shown in Figure 7a. The value of the χT product at room temperature (8.9 cm^3 K mol^{-1}) corresponds to three uncoupled spin carriers: two copper(II) ions ($S = 1/2$) and one gadolinium(III) ion ($S = 7/2$) (expected value of 8.625 cm^3 K mol^{-1} for $g = 2$). As the temperature is lowered, χT increases and reaches a maximum of 12.1 cm^3 K mol^{-1} at 9 K. This behavior indicates the presence of dominating ferromagnetic interactions likely between Gd^{III} and Cu^{II} metal ions inducing an $S = 9/2$ spin ground state for this heterometallic unit. Below 9 K, χT decreases as a result of intermolecular antiferromagnetic interactions. The interpretation of these magnetic properties is straightforward because it contains Cu^{II} and Gd^{III} spin carriers. Gadolinium(III), with a ground term $^8S_{7/2}$, has no orbital contribution and therefore can be considered as an isotropic $S = 7/2$ spin. Hence, for such compounds, the magnetic behavior can be analyzed by using the Hamiltonian

$$H = -JS_{Gd}(S_{Cu1} + S_{Cu2}) \qquad (1)$$

where S_i respresents the spin operators ($S = 1/2$ for the Cu^{II} ions and $S = 7/2$ for Gd^{III}) and J represents the magnetic

interaction between Cu and Gd metal ions. The application of the van Vleck equation[31] to the Kambe's vector coupling scheme[32] allows us to determine an analytical expression of the magnetic susceptibility in the low-field approximation

$$\chi T = \frac{Ng^2\mu_B^2}{2k_B} \frac{(35 + 84(\exp(9J/2k_BT) + \exp(7J/2k_BT)) + 165\exp(8J/k_BT))}{(6 + 8(\exp(9J/2k_BT) + \exp(7J/2k_BT)) + 10\exp(8J/k_BT))} \qquad (2)$$

Additional intertrimer interactions mediated by the diamagnetic spacers have been introduced in the frame of the mean-field approximation.[33] The experimental data are remarkably well fitted to this Heisenberg model with $g = 2.02(1)$, $J/k_B = 6.9(1)$ cm^{-1} (+9.9 K) and $zJ'/k_B = -0.03(1)$ cm^{-1} (−0.05 K) (Figure 7a). The J value is close to the one we found with another 1D compound containing the same trinuclear node.[17] The ferromagnetic interaction between the Cu^{II} and Gd^{III} metal ions leads to an $S = 9/2$ spin ground state that is also confirmed by magnetization versus field measurements at 2 K. Indeed, the experimental points follow the expected $S = 9/2$ Brillouin function with $g = 2.00(5)$ (inset Figure 7a).

The room-temperature χT product for compound **4** (9.8 cm^3 K mol^{-1}) is close to the expected value (9.75 cm^3 K mol^{-1}) for the uncoupled spin carriers (two Cu^{II}, one Gd^{III}, and three [Ni(mnt)$_2$]$^{\bullet-}$ ions), but it is definitely higher than the one (8.625 cm^3 K mol^{-1}) corresponding only to Cu^{II} and Gd^{III} ions (Figure 7b). This result seems to indicate that the [Ni(mnt)$_2$]$^{\bullet-}$ ions are magnetically active at room temperature, even if their room-temperature paramagnetism is probably reduced by inter-radical antiferromagnetic interactions present in the two types of 1-D stacks (Figure 4) as

(31) van Vleck, J. H. *The Theory of Electric and Magnetic Susceptibilty*; Oxford University Press: Oxford, U.K., 1932.
(32) Kambe, K. *J. Phys. Soc. Jpn.* **1963**, *5*, 48.
(33) The following definition of the susceptibility has been used: $\chi = \chi_{trimer}/(1 - (zJ')/(Ng^2\mu_B^2)\chi_{trimer})$. For example, see: (a) Myers, B. E.; Berger L.; Friedberg, S. *J. Appl. Phys.* **1969**, *40*, 1149. (b) O'Connor, C. J. *Prog. Inorg. Chem.* **1982**, *29*, 203.
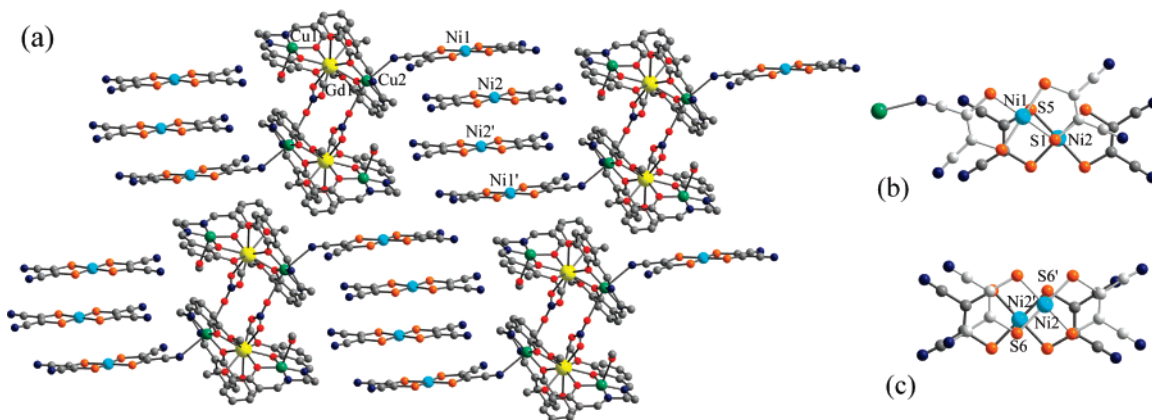
Figure 6. Packing diagram for compound **7**, showing the association of the [Ni(mnt)$_2$]$^-$ ions into supramolecular tetramers (a), and details of the interactions between the [Ni(mnt)$_2$]$^-$ anions (b and c).
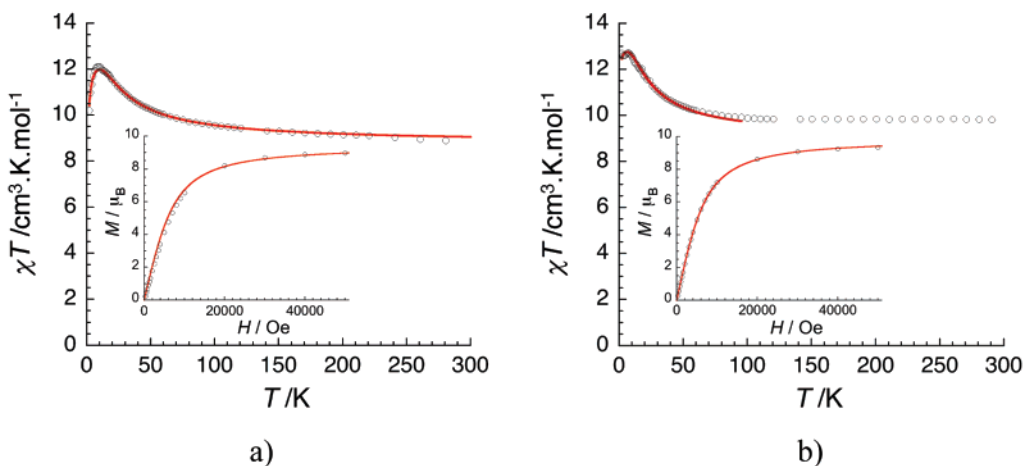
Figure 7. χT vs T plot at 500 Oe (with $\chi = M/H$ normalized per mole). Inset: M vs H plot measured at 2 K for the compounds **1** (a) and **4** (b).

shown by the extended Hückel calculations (vide supra). When the product is cooled, χT remains roughly constant down to 100 K, and then it increases and reaches a maximum of 12.7 cm^3 K mol^{-1} at 7 K. This value is close to 12.375 cm^3 K mol^{-1} value that is expected for an $S = 9/2$ spin unit (considering the ferromagnetic coupling of the Cu^{II} and Gd^{III} ions) suggesting that the [Ni(mnt)$_2$]$^{\bullet-}$ radicals become magnetically silent at low temperatures because of the antiferromagnetic interactions evoked above. The hypothesis is reinforced by the M versus H data at 2 K that are very well fitted to an $S = 9/2$ Brillouin function with $g = 2.02$-(5) (inset Figure 7b). The similarity between the experimental data shown in Figure 7 for compounds **1** and **4**, that is, the increase of the χT product synonym of dominant ferromagnetic interactions, shows clearly that the magnetism of the [Cu$_2$Gd] moieties seems to dominate the global magnetic behavior of **4**. Therefore, below 100 K (in the temperature region at which the radical are likely magnetically silent), the χT versus T plot has been fitted to eq 2, as for **1**, to roughly estimate the Cu−Gd magnetic interaction. Indeed, the experimental data are really well reproduced by the above model with $g = 2.04(1)$, $J/k_B = 5.9(1)$ cm^{-1} (+8.5 K), and $zJ'/k_B = -0.007(2)$ cm^{-1} (−0.01 K) (Figure 7b). Note that the intercomplex magnetic interactions (zJ') have been introduced in the model to reproduce the slight χT product decrease below 7 K. It is worth noting that the obtained J

value is close to the one estimated in **1** and also the one in related compounds.[17]

Let us discuss now the magnetic properties of compound **6**. At room temperature, the χT product is 15.7 cm^3 K mol^{-1} that is in agreement with the presence of one Tb^{III} (4f^8, $J = 6$, $S = 3$, $L = 3$, ^{7}F$_6$, $C = 11.82$ cm^3 K mol^{-1})[34] ion, two $S = 1/2$ Cu^{II} ions, and three $S = 1/2$ [Ni(mnt)$_2$]$^{\bullet-}$ species (Figure 8). While the temperature decreases, the χT product continuously increases to reach 19.9 cm^3 K mol^{-1} between 6 and 1.8 K indicating dominant ferromagnetic interactions within the trinuclear cation. The fitting of the experimental data with a Curie−Weiss law down to 25 K leads to $C = 15.5$ cm^3 K mol^{-1} and $\theta = +3.6$ K, thus confirming the presence of Tb^{III}−Cu^{II} ferromagnetic interaction as already observed in related compounds.[35] The magnetization measurements from 2 to 5 K, done as a function of the field reveal a lack of saturation even at 7 T (Figure 8).

M increases first rapidly below 1 T, up to 7 μ_B, and thus reaches 8.4 μ_B at 7 T almost linearly. This high-field behavior shows the presence of a significant anisotropy that prevents,

(34) Benelli, C.; Gatteschi, D. *Chem. Rev.* **2002**, *102*, 2369.
(35) (a) Osa, S.; Kido, T.; Matsumoto, N.; Re, N.; Pochaba, A.; Mrozinski, J. *J. Am. Chem. Soc.* **2004**, *126*, 420. (b) Kahn, M. L.; Mathonière, C.; Kahn, O. *Inorg. Chem.* **1999**, *38*, 3692. (c) Costes, J.-P.; Clemente-Juan, J. M.; Dahan, F.; Milon, J. *Inorg. Chem.* **2004**, *43*, 8200−8202. (d) Costes, J.-P.; Dahan, F.; Wernsdorfer, W. *Inorg. Chem.* **2006**, *45*, 5.
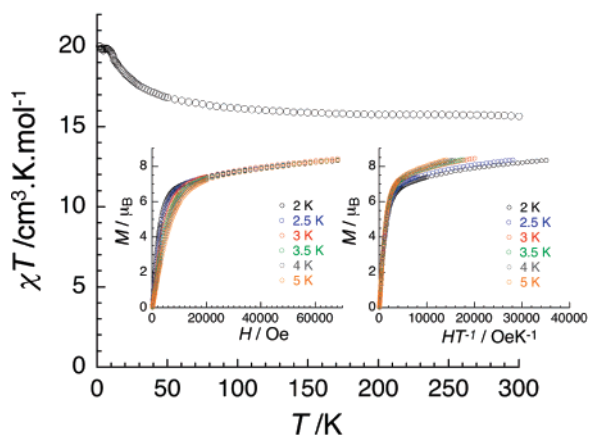
Figure 8. χT vs T plot at 1000 Oe (with $\chi = M/H$ normalized per mol). Inset: M vs H and M vs H/T plots measured between 2 and 5 K for **6**.
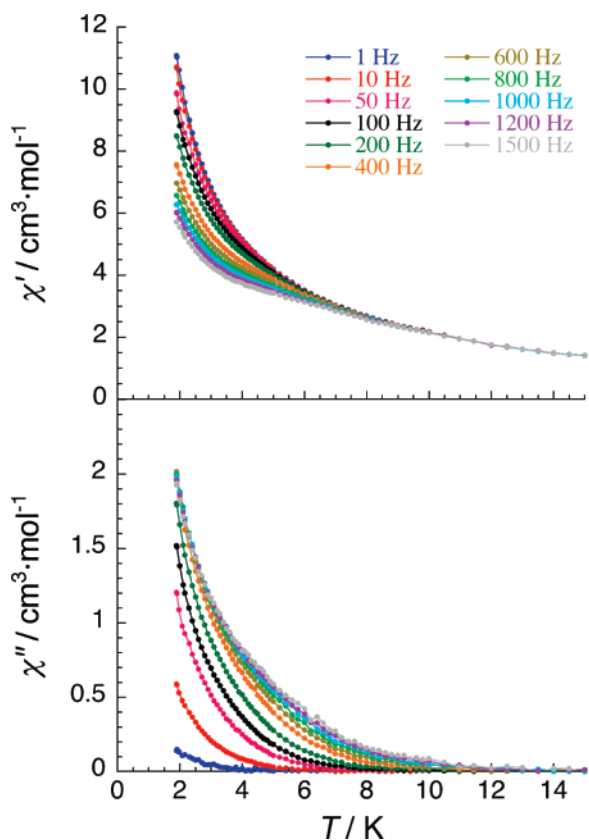
Figure 9. Temperature dependence of the ac susceptibility in zero dc field for **6** measured between 1.8 and 15 K. Top: In-phase component (χ'). Bottom: Out-of-phase component (χ'').

below 7 T, saturation of the magnetization at 11 μ_B as expected for one Tb^{III} and two Cu^{II} metal ions. Moreover the presentation of the data as an M versus H/T plot confirms the presence of anisotropy because the data are not all superposed on a single master curve.

Because of the presence of a significant magnetic anisotropy and high-spin Tb$_2$Cu units, the signature of slow relaxation of the magnetization or single-molecule magnet (SMM) behavior has been checked by ac susceptibility measurements. In zero-dc field, frequency-dependent ac susceptibility is observed below 10 K (Figure 9). The shape of this relaxation process is broad and does not look like a
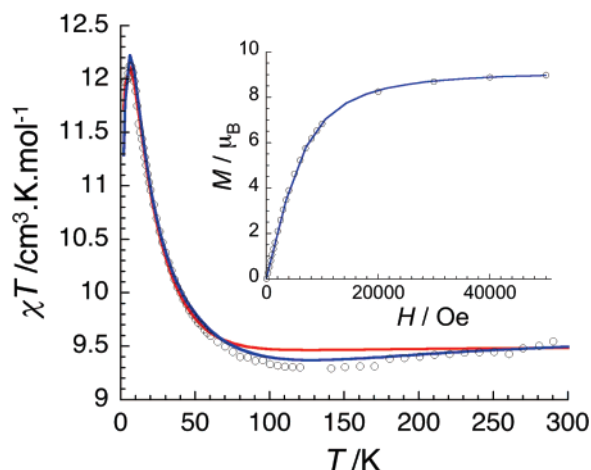
Figure 10. χT vs T plot at 500 Oe for the compound **7** calculated for one unit GdCu$_2$Ni$_3$. Simulations within the model given in eq 3 are shown for $J_1 = 5$ cm^{-1}, $J_2 = -10$ cm^{-1}, $J_3 = -150$ cm^{-1}, $zJ' = -0.01$ cm^{-1}, $g = 2.02$ (red line) and $J_1 = 4.3$ cm^{-1}, $J_2 = -10$ cm^{-1}, $J_3 = -250$ cm^{-1}, $zJ' = -0.025$ cm^{-1}, $g = 2.2$ (blue line). Inset: M vs H data at 2 K for **7**, calculated for one unit GdCu$_2$Ni$_3$. Note that the fit of the experimental data using an $S = 9/2$ Brillouin function leads to a virtually identical result with $g = 2.00(5)$.

classical SMM behavior with a single relaxation process. A distribution of relaxation time might be present because of, for example, structural disorder, defects, or different intermolecular magnetic interactions. In conclusion, this compound is probably a SMM, but the observed magnetization relaxation is far from the archetype SMM behavior; therefore, it is not possible to extract its characteristic relaxation time from the obtained ac susceptibility measurements.

The χT versus T curve for the compound **7** is given in Figure 10. The high-temperature limit of the χT product for a {Cu$_2$GdNi$_2$} unit (9.6 cm^3 K mol^{-1}), corresponds well to five uncoupled spin carriers (expected value of 9.375 cm^3 K mol^{-1} with an average g value of 2): two [Ni(mnt)$_2$]$^-$ species ($S = 1/2$), two copper(II) ions ($S = 1/2$), and one gadolinium(III) ion ($S = 7/2$). When the temperature is lowered, the χT product slightly decreases to 9.3 cm^3 K mol^{-1} at 120 K and then increases to reach a maximum at 6 K of around 12.1 cm^3 K mol^{-1}. The latter observation is similar to that for **1** and **4** and reveals the presence of dominant ferromagnetic interactions within the trinuclear cation. Below 6 K, the final decrease of the χT product is probably related to intermolecular antiferromagnetic interactions.

Magnetization versus field measurements at 2 K (Figure 10) show the saturation value of 8.97 μ_B, corresponding well to an $S = 9/2$ ground-state spin for the {Cu$_2$GdNi$_2$} unit. As in **4**, the [Ni(mnt)$_2$]$^{\bullet-}$ radicals seems to be magnetically silent at low temperatures because of strong antiferromagnetic interactions between radicals. This result is confirmed by the M versus H data at 2 K, which are very well fitted to an $S = 9/2$ Brillouin function with $g = 2.00(5)$.

The structural similarity of the CuGdCu units in **1** and **7** allows us to assume similar exchange interactions between gadolinium and copper ions (J_1) and close values of g for Cu in these two compounds. The most important exchange coupling between CuGdCu units and their neighbors is expected to be that with the semi-coordinated [Ni1(mnt)$_2$]$^-$
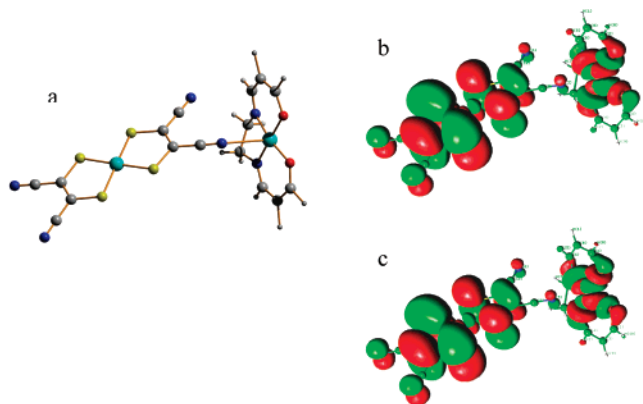
Figure 11. Structure of the Cu2Ni1 fragment of compound **7** used in the ab initio calculations (a) and the active orbitals φ_1 (b) and φ_2 (c) obtained in the (2i4) CASSCF calculation.

(Figure 6). To estimate the corresponding exchange parameter (J_2), we performed CASSCF/CASPT2 calculations[36] of the lowest-spin states in a binuclear fragment Ni1Cu2 (Figure 11a). Within the active space (2i4), the CASPT2 total energy for the ground-state singlet of this fragment is 2.3 cm^{-1} lower than that for the ground-state triplet, which means that the exchange interaction is weakly antiferromagnetic ($J_2 = -2.3$ cm^{-1}). The wave functions for the singlet and triplet states are obtained almost completely of the form $|\varphi_1\bar{\varphi}_1 - \varphi_2\bar{\varphi}_2|/\sqrt{2}$ and $|\varphi_1\varphi_2|$, respectively, where the active molecular orbitals φ_1 and φ_2 are shown in Figures 11b and c, respectively. These molecular orbitals represent bonding and antibonding combinations of magnetic orbitals centered on the copper fragment (φ_{Cu}) and on the [Ni1(mnt)$_2$]$^-$ unit (φ_{Ni}). In terms of these magnetic orbitals, containing one unpaired electron each, the singlet and triplet wave functions can be written in a more familiar form as $|\varphi_{Cu}\bar{\varphi}_{Ni} - \bar{\varphi}_{Cu}\varphi_{Ni}|/\sqrt{2}$ and $|\varphi_{Cu}\varphi_{Ni}|$, respectively.

We can see from Figure 11 that φ_{Cu} is of the copper d$_{x^2-y^2}$ type strongly hybridized with the σ orbitals of surrounding oxygen and nitrogen atoms, while φ_{Ni} is predominantly of the π sulfur type. There is a non-negligible π electron density on the nitrogen atom of the [Ni1(mnt)$_2$]$^-$ unit bounded to copper. The corresponding N−Cu bond deviates by several degrees from the normal to the plane of the d$_{x^2-y^2}$ orbital, which causes their π hybridization and leads to antiferromagnetic interaction between the unpaired electrons on the [Ni1(mnt)$_2$]$^-$ and Cu units. Enlarging the active space to (10i8) increases the exchange interaction dramatically ($J_2 = -116$ cm^{-1}). The analysis of the ground-state wave function shows that, in addition to the singlet configuration of φ_1 and φ_2 active orbitals, which did not change much compared to the previous calculation, additional configurations arising from two-electron excitation from doubly occupied to empty orbitals become admixed. Actually, it is known that sulfur orbitals hybridize strongly to the orbitals of transition metals like copper and nickel; therefore an adequate active space should include all molecular orbitals generated by 3p orbitals

on sulfur atoms.[37] Such an active space would be much larger than the (10i8) one we used, as a consequence, we cannot claim quantitative accuracy for the calculated values of J_2. Although calculations with larger active spaces would be impractical, the tendency for antiferromagnetic coupling in the Cu2Ni1 fragment clearly emerges from our calculations, and a value on the order of ten wavenumbers for J_2 seems to be quite realistic. Finally, the exchange interaction between Ni1 and Ni2 species (J_3) is expected to be antiferromagnetic and very strong, according to the above estimation of the effective transfer parameter ($\beta_{HOMO-HOMO} = 0.430$ eV). Indeed, for any guess for the electron repulsion parameter (U), the antiferromagnetic contribution to the exchange parameter, $-4\beta^2/U$,[38] is expected to be on the order of hundreds of wavenumbers. On the other hand, the next-neighbor exchange interactions (Ni2−Ni2′ and Cu−Gd between neighboring Cu$_2$Gd units) are expected to be much weaker.

Thus the exchange model considering the three interactions discussed above can be defined as

$$H = -J_1[S_{Cu1}S_{Gd} + S_{Gd}S_{Cu2}] + J_2 S_{Cu2}S_{Ni1} + J_3 S_{Ni1}S_{Ni2} \quad (3)$$

with the remaining exchange interactions being described by the mean-field parameter zJ'.[33] For the average g factor of the metal ions, we took the value obtained for the compound **1**. The best simulations of magnetic susceptibility and magnetization curves are shown in Figure 10 by red and blue continuous lines that correspond to the following set of parameters: $J_1 = 5$ cm^{-1}, $J_2 = -10$ cm^{-1}, $J_3 = -150$ cm^{-1}, $zJ' = -0.01$ cm^{-1}, $g = 2.02$ (red line) and $J_1 = 4.3$ cm^{-1}, $J_2 = -10$ cm^{-1}, $J_3 = -250$ cm^{-1}, $zJ' = -0.025$ cm^{-1}, $g = 2.2$ (blue line). A satisfactory simulation of the data at high temperatures (above 120 K) was never obtained. To obtain a more pronounced dip of χT at 100 K, one should increase Ni1−Ni2 antiferromagnetic exchange and the copper g factor, which also will increase the high-temperature limit of χT. The corresponding simulation, shown in Figure 10 by a blue line, follows the experiment better, although the susceptibility above 120 K is still poorly reproduced. The reason for this discrepancy is unclear. Because of a strong antiferromagnetic coupling between Ni1 and Ni2 species, bounding their $S = 1/2$ spins into a singlet, Cu$_2$GdNi$_2$ units possess an effective $S = 9/2$ spin ground state in agreement with the M versus H data (vide supra, Figure 10). The χT versus T plot has also been fitted to eq 2, as for **4**, considering that below 100 K the radical anions are likely already strongly antiferromagnetically coupled and thus magnetically silent. Indeed the experimental data below 100 K are well reproduced by this simplified approach with $g = 2.02(1)$, $J/k_B = +4.8(1)$ cm^{-1} (+6.9 K), and $zJ'/k_B = -0.010(5)$ cm^{-1} (−0.014 K). As expected, the obtained J value is close to the one estimated in **1** and **4** and also in related compounds.[17]

Conclusion

The results presented herein illustrate that 3p−3d−4f heterospin systems can be obtained by employing

(36) Karlström, G.; Lindh, R.; Malmqvist, P.-Å.; Roos, B. O.; Ryde, U.; Veryazov, V.; Widmark, P.-O.; Cossi, M.; Schimmelpfennig, B.; Neogrady, P.; Seijo, L. *Comput. Mater. Sci.* **2003**, *28*, 222.

(37) Azizi, Z.; Roos, B. O.; Veryazov, V. *Phys. Chem. Chem. Phys.* **2006**, *8*, 2727.

(38) Kahn, O. *Molecular Magnetism*; VCH Publishers: New York, 1993.

[Ni(mnt)$_2$]$^{q-}$ anions and [Cu$_2$Ln]$^{3+}$ cations as tectons. These results, together with those we have previously reported, show that the oligonuclear 3d−4f species, [CuLn]$^{3+}$ and [Cu$_2$-Ln]$^{3+}$, are extremely useful starting materials in the design of complexes containing three different spin carriers (2p−3d−4f, 3d−3d′−4f, 3p−3d−4f). The nickel dithiolene species act either as ligands toward the copper ions or can be found uncoordinated in the crystal lattice. The anionic radicals are strongly antiferromagnetically coupled at low temperatures as a consequence of their tendency to stack in the crystal, regardless of their function, coordinated or uncoordinated, yet their contribution to the global magnetism is visible in the high-temperature regime.

Experimental Section

Synthesis. The mononuclear [Cu(H$_2$O)L^1] and [CuL^2] and dinuclear precursors [{Cu(H$_2$O)L^1}Ln(O$_2$NO)$_3$] and [{CuL^2}Ln(O$_2$-NO)$_3$] (L^1 = *N,N′*-propylene-di(3-methoxysalicylideneiminato), L^2 = *N,N′*-ethylene-di(3-methoxysalicylideneiminato)) were obtained by following the general procedure reported by Costes et al.[15] The bis(dithiolene) complexes, (TBA)$_2$[Ni(mnt)$_2$] and (TBA)[Ni(mnt)$_2$] (TBA = *n*-tetrabutylammonium), have been obtained according to Davison et al.[39]

Synthesis of $^1_\infty$[{CuL^1}$_2$Gd(O$_2$NO){Ni(mnt)$_2$}]·CH$_3$OH·CH$_3$CN (1). [Cu(H$_2$O)L^1] (0.1 mmol) and [{Cu(H$_2$O)L^1}Gd(O$_2$NO)$_3$] (0.1 mmol) were dissolved in 10 mL of a acetonitrile−methanol (1:1) mixture and was stirred for 20 min. To this solution was added 10 mL of a solution containing 0.1 mmol of (TBA)$_2$[Ni(mnt)$_2$] in acetonitrile. The slow evaporation at room temperature of the resulting mixture affords **1** as brown crystals. The crystals were filtered and washed with a mixture of methanol−ethyl ether (1 : 2). Yield: 88%. Elemental chemical analyses: 40.86 C; 3.35 H; 9.70 N (found); 40.89 C; 3.29 H; 9.73 N (calcd).

Synthesis of $^1_\infty$[{CuL^1}$_2$Sm(O$_2$NO){Ni(mnt)$_2$}]·2CH$_3$CN (2). Compound **2** was obtained in the same manner as **1**, using [{Cu-(H$_2$O)L^1}Sm(O$_2$NO)$_3$] instead of [{CuL^1}Gd(O$_2$NO)$_3$]. Yield: 85%. Elemental chemical analyses: 41.35 C; 3.30 H; 10.33 N (found); 41.66 C; 3.22 H; 10.69 N (calcd).

Synthesis of [{(CH$_3$OH)CuL^2}$_2$Sm(O$_2$NO)][Ni(mnt)$_2$] (3). [CuL^2] (0.1 mmol) and [{CuL^2}Sm(O$_2$NO)$_3$] (0.1 mmol) were dissolved in 10 mL of acetonitrile−methanol (1:1), and the mixture was stirred for 20 min. To this solution was added 10 mL of a solution containing 0.1 mmol of (TBA)$_2$[Ni(mnt)$_2$] in acetonitrile. The slow evaporation at room temperature of the resulting mixture affords **3** as brown crystals. The crystals were filtered and washed with a mixture of methanol−ethyl ether (1 : 2). Yield: 85%. Elemental chemical analyses: 39.43 C; 3.24 H; 9.40 N (found); 39.65 C; 3.04 H; 9.05 N (calcd).

Synthesis of [{(CH$_3$CN)CuL^1}$_2$Gd(H$_2$O)][Ni(mnt)$_2$]$_3$·2CH$_3$CN (4). [Cu(H$_2$O)L^1] (0.1 mmol) and [{Cu(H$_2$O)L^1}Gd(O$_2$NO)$_3$] (0.1 mmol) were dissolved in 10 mL of acetonitrile−methanol (1:1), and the mixture was stirred for 20 min. To this solution was added 15 mL of a solution containing 0.3 mmol of (TBA)[Ni(mnt)$_2$] in acetonitrile. The slow evaporation at room temperature of the resulting mixture affords **4**. The crystals were filtered and washed with a mixture of methanol−ethyl ether (1:2). Yield: 75%. Elemental chemical analyses: 39.25 C; 2.68 H; 12.77 N (found); 38.88 C; 2.42 H; 12.95 N (calcd).

Synthesis of [{(CH$_3$CN)CuL^1}$_2$Sm(H$_2$O)][Ni(mnt)$_2$]$_3$·2CH$_3$CN (5). Compound **5** was obtained in the same manner as **4**, using

[{Cu(H$_2$O)L^1}Sm(O$_2$NO)$_3$] instead of [{CuL^1}Gd(O$_2$NO)$_3$]. Yield: 70%. Elemental chemical analyses: 39.38 C; 2.76 H; 12.77 N (found); 39.00 C; 2.43 H; 13.00% N (calcd).

Synthesis of [{(CH$_3$CN)CuL^1}$_2$Tb(H$_2$O)][Ni(mnt)$_2$]$_3$·2CH$_3$CN (6). [Cu(H$_2$O)L^1] (0.2 mmol) and Tb(NO$_3$)$_3$ (0.1 mmol) were stirred for 30 min in 10 mL of acetonitrile−methanol (1:1). To this solution was added 15 mL of solution containing 0.3 mmol of (TBA)[Ni-(mnt)$_2$] in acetonitrile, and the resulting mixture was left to evaporate at room temperature. Dark blue (black) crystals of **6** were formed after 2 days. Yield: 77%. Elemental chemical analyses: 38.97 C; 2.28 H; 13.23 N (found); 38.85 C; 2.42 H; 12.94 N (calcd).

Synthesis of [{(CH$_3$OH)CuL^2}{CuL^2}Gd(O$_2$NO){Ni(mnt)$_2$}]-[Ni(mnt)$_2$]·CH$_2$Cl$_2$ (7). [CuL^2] (0.1 mmol) and [{CuL^2}Gd(O$_2$-NO)$_3$] (0.1 mmol) were dissolved in 15 mL of methanol, and the mixture was stirred for 30 min. To this solution was added 15 mL of a solution containing 0.3 mmol of (TBA)[Ni(mnt)$_2$] in CH$_2$Cl$_2$. The slow evaporation at room temperature of the resulting mixture affords **7** as small black crystals. The crystals were filtered and washed with a mixture methanol−ethyl ether (1:2). Yield: 70%. Elemental chemical analyses: 35.97 C; 2.66 H; 10.33 N (found); 36.17 C; 2.30 H; 10.15 N (calcd).

X-ray Crystallography. Details about data collection and solution refinement are given in Table 2. X-ray diffraction measurements were performed on a Bruker Kappa CCD diffractometer for **1**, **3**, **4**, **6**, and **7** and on a STOE Imaging Plate System for **2** and **5**, both operating with a Mo Kα (λ = 0.71073 Å) X-ray tube with a graphite monochromator. The structures were solved (SHELXS-97) by direct methods and refined (SHELXL-97) by full-matrix least-square procedures on F^2.[40] All non-H atoms were refined anisotropically. The CCDC reference numbers are 650040−650046.

Magnetic Measurements. The magnetic susceptibility measurements for **1**, **4**, and **7** were obtained with the use of a Quantum Design SQUID magnetometer. The magnetic susceptibility measurements for **6** were obtained with the use of a Quantum Design SQUID magnetometer MPMS-XL. This magnetometer works between 1.8 and 400 K for dc applied fields ranging from −7 to 7 T. The ac susceptibility measurements have been performed with an oscillating ac field of 3 Oe and ac frequencies ranging from 1 to 1500 Hz. The magnetic data were corrected for the diamagnetic contribution of the samples, estimated using the Pascal's constants, and the sample holders.

Theoretical Calculations. The overlap interaction energies $\beta_{\text{HOMO−HOMO}}$ were of the extended-Hückel type.[29a,b] A modified Wolfsberg−Helmholtz formula was used to calculate the non-diagonal H$_{\mu\nu}$ values.[41] Double-ζ Slater-type orbitals for C, S, N, and Ni were used.[42]

The magnetic interaction between the [Ni1(mnt)$_2$]$^-$ unit and the Cu2 fragment (copper ion with its immediate environment), where hydrogen atoms have been introduced to saturate the dangling bonds on the peripheral carbons (Figure 11a), have been investigated by CASSCF/CASPT2 quantum-chemistry calculations with the latest relativistic basis sets: ANO-RCC [5s4p2d] for Cu, Ni, [4s3p] for S,[3s,2p] for C,N,O, and [2s] for H, as implemented in MOLCAS, version 6.4, package.[36] The geometry of the fragment was taken from the experimental one (Figure 5). The CASSCF wave functions used in the subsequent perturbation treatment were obtained by

(39) Davison, A.; Holm, R. H. *Inorg. Synth.* **1967**, *10*, 8.

(40) Sheldrick, G. M. *Programs for the Refinement of Crystal Structures*; University of Göttingen: Göttingen, Germany, 1996.

(41) Ammeter, J. H.; Bürgi, H.-B.; Thibeault, J.; Hoffmann, R. *J. Am. Chem. Soc.* **1978**, *100*, 3686.

(42) Clementi, E.; Roetti, C. *At. Data Nucl. Data Tables* **1974**, *14*, 177.

Table 2. Crystallographic Data, Details of Data Collection, and Structure Refinement Parameters for Compounds **1** − **7**

	1	2	3
chemical formula	$C_{49}H_{47}Cu_2GdN_{10}NiO_{12}S_4$	$C_{50}H_{46}Cu_2N_{11}NiO_{11}S_4Sm$	$C_{46}H_{42}Cu_2N_9NiO_{13}S_4Sm$
M (g mol^{-1})	1439.19	1441.31	1393.27
temp (K)	293(2)	293(2)	293(2)
wavelength (Å)	0.71073	0.71073	0.71073
cryst syst	monoclinic	monoclinic	monoclinic
space group	$C2/c$	$C2/c$	$P21/c$
a (Å)	27.0698(15)	27.189(5)	22.9525(12)
b (Å)	11.6894(10)	11.293(2)	8.1734(5)
c (Å)	18.1500(10)	18.569(4)	29.7656(13)
α (deg)	90	90	90
β (deg)	95.481(7)	96.50(3)	105.240(7)
γ (deg)	90	90	90
V (Å^3)	5716.9(7)	5665(2)	5387.7(5)
Z	4	4	4
D_c (g cm^{-3})	1.664	1.683	1.718
μ (mm^{-1})	2.416	2.304	2.421
$F(000)$	2856	2868	2788
GOF on F^2	0.984	0.989	1.014
final R1, wR2 [$I > 2\sigma(I)$]	0.0439, 0.0787	0.0328, 0.0572	0.0432, 0.0860
R1, wR2 (all data)	0.1026, 0.0946	0.0816, 0.0701	0.0811, 0.1016
largest diff. peak and hole (e Å^{-3})	0.686, −0.687	0.603, −0.407	0.848, −0.796

	4	5	6	7
chemical formula	$C_{70}H_{52}Cu_2GdN_{20}Ni_3O_9S_{12}$	$C_{70}H_{52}Cu_2N_{20}Ni_3O_9S_{12}Sm$	$C_{70}H_{52}Cu_2N_{20}Ni_3O_9S_{12}Tb$	$C_{54}H_{41}Cl_2Cu_2GdN_{13}Ni_2O_{12}S_8$
M (g mol^{-1})	2162.50	2155.60	2164.17	1793.13
temp (K)	293(2)	293(2)	293(2)	293(2)
wavelength (Å)	0.71073	0.71073	0.71073	0.71073
cryst syst	triclinic	triclinic	triclinic	triclinic
space group	$P\bar{1}$	$P\bar{1}$	$P\bar{1}$	$P\bar{1}$
a (Å)	10.6774(7)	10.6526(7)	10.6377(14)	15.1036(11)
b (Å)	14.7463(8)	14.7961(10)	14.7649(16)	15.9640(16)
c (Å)	30.3722(12)	30.414(2)	30.375(3)	16.1965(11)
α (deg)	100.534(8)	100.438(8)	100.543(8)	87.921(8)
β (deg)	94.115(7)	94.291(8)	94.058(10)	76.006(8)
γ (deg)	109.356(8)	109.418(7)	109.364(9)	62.802(8)
V (Å^3)	4390.4(4)	4398.8(5)	4380.3(9)	3357.8(5)
Z	2	2	2	2
D_c (g cm^{-3})	1.636	1.627	1.641	1.774
μ (mm^{-1})	2.199	2.109	2.254	2.544
$F(000)$	2164	2160	2166	1784
GOF on F^2	0.896	0.798	0.979	0.930
final R1, wR2 [$I > 2\sigma(I)$]	0.0743, 0.0774	0.0451, 0.0979	0.0788, 0.1342	0.0599, 0.0866
R1, wR2 (all data)	0.2937, 0.1090	0.1735, 0.1366	0.2065, 0.1729	0.1950, 0.1112
largest diff. peak and hole (e Å^{-3})	0.600, −0.608	0.718, −1.932	1.064, −1.082	1.153, −0.607

choosing first a minimal active space of two electrons in four active orbitals, designated as (2i4) (including singly occupied orbitals plus their double shell counterparts). A more extended active space of 10 electrons in 8 orbitals (10i8) has been designed in such a way that the bridging orbitals enter into the active space as well. The inclusion of bridging orbitals into the active space was found in many cases to be important for the correct description of the exchange interactions.[43] The dynamical electron correlation was described at the CASPT2 level by correlating the valence electrons of all atoms plus the 3p electrons of Cu and Ni. The relativistic effects were taken into account by evaluating the mass-velocity correction and the one-electron Darwin contact term for the CASSCF wave functions.

(43) de Graaf, C.; Sousa, C.; Moreira, I. P. R.; Illas, F. *J. Phys. Chem. A* **2001**, *105*, 13171.